



ACADEMIC
PRESS

Available online at www.sciencedirect.com

SCIENCE @ DIRECT®

NeuroImage

NeuroImage 19 (2003) 132–144

www.elsevier.com/locate/ynimg

The spatial extent of the BOLD response

Ziad S. Saad,^{a,b,*} Kristina M. Ropella,^b Edgar A. DeYoe,^c and Peter A. Bandettini^a

^a *Laboratory of Brain and Cognition, National Institute of Mental Health, NIH, Bethesda, MD 20892-1148, USA*

^b *Department of Biomedical Engineering Marquette University, Milwaukee, WI 53233, USA*

^c *Department of Cell Biology, Neurobiology and Anatomy, Medical College of Wisconsin, Milwaukee, WI 53226, USA*

Received 16 August 2002; revised 29 October 2002; accepted 21 November 2002

Abstract

Functional magnetic resonance imaging is routinely used to localize brain function, with multiple brain scans averaged together to reveal activation volumes. In this study, we examine the seldom-studied effect of multiple scan averaging on the extent of activation volume. Using restricted visual field stimulation, we obtained a large number of scan repetitions and analyzed changes in activation volume with progressively increased averaging and across single scans. Activation volume increased monotonically with averaging and failed to asymptote when as many as 22 scans were averaged together. Expansions in the spatial extent of activation were not random; rather, they were centered about activation loci that appear with little or no averaging. Using empirical and simulated data, changes with averaging in activation volumes and cross correlation coefficient distributions revealed the presence of considerably more activated voxels than commonly surmised. Many voxels have low SNR and remain undetected without extensive averaging. The primary source of such voxels was not downstream venous drainage since there was no significant and consistent delay difference between voxels activated at different averaging levels. Voxels with low SNR may reflect a diffuse subthreshold activity centered about spiking neurons, dephasing gradients from distal veins, or simply a blood flow response extending beyond the locus of neuronal firing. Across single scans, as much as twofold changes in activation volume were observed. These changes were not correlated with the order of scan acquisition, subject task performance, or signal and noise properties of activated voxels. Instead, they may reflect subtle changes between overlapping noise and signal frequency components.

© 2003 Elsevier Science (USA). All rights reserved.

Keywords: Activation volume; Functional magnetic resonance imaging; Visual cortex; MRI methods/techniques

Introduction

Functional magnetic resonance imaging (fMRI) is a widely used method for mapping human brain function. Through coupling mechanisms that remain a subject of debate, neuronal stimulation induces hemodynamic changes that are detectable by blood oxygenation level-dependent (BOLD) MRI (Bandettini and Ungerleider, 2001; Logothetis et al., 2001; Magistretti, 2000; Magistretti et al., 1999; Ogawa et al., 1990a; Villringer, 1997; Villringer and Dirnagl, 1995). To date, many studies of BOLD signal

properties have focused on its temporal dynamics and linearity and hemodynamic and biophysical models (Arthurs et al., 2000; Bandettini and Wong, 1997; Bandettini et al., 1992; Birn et al., 2001; Boynton et al., 1996; Buxton, 2001; Buxton et al., 1998; Davis et al., 1998; Duong et al., 2000; Friston et al., 1998; Hoogenraad et al., 2001; Kim et al., 1999; Kim and Ugurbil, 1997; Kruggel and von Cramon, 1999a, 1999b; Kwong et al., 1992; Lee et al., 1995; Liu and Gao, 2000; Mandeville et al., 1998, 1999; Marota et al., 1999; Menon et al., 1993; Miller et al., 2001; Ogawa et al., 1990a, 1990b; Ogawa and Lee, 1992; Saad et al., 2001; Vasquez and Noll, 1998; Yacoub et al., 1999). In addition, studies have focused on the spatial localization of the BOLD response relative to the sites of neuronal activation and the limits of its spatial resolution. (Duong et al., 2001; Engel et al., 1997; Segebarth, 1994, No. 149; Goodyear and

* Corresponding author. Statistical and Scientific Computing Core, National Institute of Mental Health, 10 Center Dr. Room 1D80, Bethesda, MD 20892-1148, USA. Fax: +1-301-402-1370.

E-mail address: ziad@nih.gov (Z.S. Saad).

Menon, 2001; Hess et al., 2000; Kim et al., 2000; Kinahan and Noll, 1999; Lai et al., 1993; Liu et al., 1999; Menon and Goodyear, 1999; Yang et al., 1997). However, few studies have addressed the spatial extent of the BOLD response to neuronal stimulation despite the use of such a metric in imaging studies (Karni et al., 1995; Krings et al., 2001).

In an fMRI scan, the signal to noise ratio (SNR) is the limiting factor in determining the full extent of brain activation. Activated voxels with low SNR may not be statistically distinguishable from inactivated counterparts. In almost all fMRI experiments, thresholds for detecting activated voxels are set to minimize false positive (type I) errors, whereby an inactive voxel is incorrectly classified as activated. The result of such high specificity for activated voxels is a loss of sensitivity, whereby an undetermined number of activated voxels go undetected (false negatives, type II error). Such type II errors result from low signal to noise ratio in the undetected active voxels, and consequently, the spatial extent of the fMRI response is underestimated. To determine the full spatial extent of the BOLD response, one needs to detect low SNR voxels (reduce type II error) without increasing the rate of false detection (keep type I error constant). This is achieved by collecting more data samples without further constraining the statistical model with presumptive information on the BOLD response or noise. Recently, Huettel and McCarthy (2001) examined the extent of the BOLD response as a function of the number of averaged single trial stimulations and found the volume of activation to increase exponentially with averaging. However, it is unclear whether such increases would occur in block design stimuli that induce much higher SNR responses when compared with single trial stimulation. Test–retest studies have shown that the extent of activation varied considerably between and across scans (Genovese et al., 1997; Manoach et al., 2001; Noll et al., 1997; Rombouts et al., 1997). The sources of variability of the spatial extent of the BOLD response remain undetermined and could range from stimulus properties to subjects' clinical conditions, attention, and learning. In this study, we examine in detail the spatial extent of the BOLD response to visual stimulation in normal volunteers by collecting multiple repetitions of the same scan and examining the extent of the BOLD response across repetitions and with increased averaging. The visual stimulus and task used were designed to minimize attention modulation and eye movement artifacts. With increased averaging, we found large changes in the activation volume and SNR distributions, which indicated that the volume of activation was considerably larger than typically surmised. To determine the source of volume variation, we searched for correlation between activation volumes and task performance, scan acquisition order, signal, and noise levels. Furthermore, we compared the delay distribution of voxels with high SNR to those with low SNR to test the hypothesis that voxels with low SNR originate in distal draining veins.

Results from this study are critical for interpreting dif-

ferences in the spatial patterns of fMRI response (Savoy, 2001) to differing stimuli, scanning sessions, or both.

Methods

Scanning parameters and visual stimulation

We used gradient echo (GE) EPI to image the BOLD response in the visual cortex. The imaged volume consisted of 18–24 axial slices 4 mm thick, an in-plane resolution of 3.75×3.75 mm, and TR = 2000 ms. Hereafter, a scan is defined as the time series of 100 volumes obtained simultaneously during one 200-s stimulus presentation period. A scanning session refers to the group of scans acquired serially with the subject's head in a constant position. High-resolution anatomical images, on which functional data were superimposed, were obtained using a FSPGR (fast spoiled gradient recalled) pulse sequence with a slice thickness between 1 and 1.2 mm and in-plane resolution of 0.94×0.94 mm. Data were obtained from three subjects (S1, S2, and S3) using 1.5-T (S1, S2) and 3-T (S1, S3) GE-Signa scanners.

The stimulus consisted of a black and white checkered annulus flickered at 8 Hz and centered on a fixation square overlaid on an equiluminant gray background. The stimulus was generated using a Cambridge Instruments VSG 2/3 video card. In a 200-s scan, the annulus was presented for 20 s (ON) followed by 20 s of fixation point only (OFF).

Spatial attention has been shown to modulate the fMRI signal even if the visual stimulus is held stationary (Brefczynski and DeYoe, 1999). Thus if subject attention is not maintained at a fixed location in the visual field, a BOLD response may be observed in areas that are not directly stimulated by the annulus. To control for spatial attention modulation that could be synchronous with stimulus presentation, we required the subjects to perform a visual task superimposed on the fixation square during the entire duration of the scan (Beauchamp et al., 1997; Kastner et al., 1998; Somers et al., 1999; Tootell et al., 1998). The task was designed to force the subjects to continuously maintain a constant attention to the fixation point. This was achieved by presenting targets for a brief duration at frequent intervals. A discrimination task was superimposed on the square during both the ON and OFF periods. For data obtained at 1.5 T, the eccentricity of the annulus covered 2.5 to 5.2°, and the fixation task consisted of detecting a change in the color of a vertical bar superimposed on the fixation point. The bar was presented every 1 s for a period of 0.3 s. The stimulus was viewed using a custom optical system designed to project images directly onto the retinæ of subjects (DeYoe et al., 1994). For data obtained at 3 T, we used annuli covering 0.9 to 2.0° (small) and 0.3 to 5.5° (large). The fixation task required the volunteer to decide whether a colored line superimposed on the fixation point was red and vertical or blue and horizontal. The target line appeared for

240 ms at random intervals varied between 700 and 1700 ms. The stimulus was projected onto a screen positioned at the subject's feet. Subjects viewed the stimulus through two prisms mounted on the RF coil, and their task responses were recorded for future analysis.

For this study, it was imperative that subjects maintain fixation throughout the scan. The discrimination task was designed in part to help achieve this. The colored line was small and presented briefly at random intervals. Thus if subjects performed saccades, they would miss the target and their performance would drop. There was also the possibility that subjects would perform the task without maintaining gaze on the fixation point. To address this, we tested the performance of two of the subjects using off-center fixation. The test was done outside the scanner and after all the fMRI data presented in this paper were collected. An off-center fixation point was placed 1.7° from the central square where the target is presented and subjects were instructed to perform the same task performed in the scanner while maintaining fixation on the off-center point.

The visual stimulus was designed to stimulate a specific region of the visual field that would translate into spatially delineated patterns of neuronal activity in early visual areas (DeYoe and Van Essen, 1988; Felleman and Van Essen, 1991). From retinotopic studies in animal and human lesion literature, it can be shown that in early visual areas, such as V1 and V2, the pattern of neural response can be predicted from the stimulus location in the visual field (Horton and Hoyt 1991). Thus it was important in our stimulus design to ensure that photic stimulation occurred in a restricted region of the visual field. To this end, we equated the average luminance over the annulus location during the ON period and at the same location during the OFF period. Luminance was measured with a high-speed photo detector (DET210, Tholabs Inc., Newton, NJ, USA). For the data collected on the 3-T scanner we also considered the possibility that scattered light from the projection screen might stimulate peripheral regions of the visual field. This could occur through average intensity modulation between the ON and OFF periods and from the 8-Hz flicker modulated by the ON–OFF stimulus cycle. To control for these artifacts, we collected data using a low stimulus contrast of 28%. This low contrast was chosen such that, with the scanner room lights turned off, subjects were not able to detect the presence or the absence of the annulus unless the projection screen was in sight. As an extra measure to ensure that subjects could not adapt to the low brightness during the experiment and detect low-intensity reflected light, the scanner room lights were turned on during the entire scanning session.

Active voxel detection, delay estimation, and scan averaging

Inter- and intrascan motion correction was performed using AFNI (Cox and Hyde, 1997). Volumes in the EPI

scans were registered to the EPI volume that was acquired immediately before or after the high-resolution FSPGR anatomical scan. This minimized motion artifacts within and across scans during an entire scanning session. We used the anterior and posterior commissure (AC, PC) landmarks to align functional data from the same subjects across scanning sessions (Talairach and Tournoux, 1988).

Activated voxels were detected, and their response delay estimated using a variant on the cross correlation method (Saad et al., 2001, 2002). The method uses the Hilbert Transform of the cross correlation function to estimate both the delay between a reference time series and the fMRI signal and the maximum cross correlation coefficient. Hence activated voxels are detected irrespective of their response delays. The reference time series used was a square wave (the stimulus' time course) convolved by the gamma-variate model of the BOLD response (Cohen, 1997). Voxels with a cross correlation coefficient >0.5 were considered activated. At the chosen cross correlation threshold and assuming temporally and spatially uncorrelated noise, the type I error is estimated at $P < 0.0001$, with Bonferroni correction. The presence of autocorrelation in the fMRI noise may result in P values that are higher than estimated. On the other hand, the Bonferroni correction for repeated sampling results in a conservative estimate of P due to the spatial correlation of fMRI noise. However, even if the conservative Bonferroni correction did not offset the autocorrelation effect, P would be as high as 0.00015, which is still highly significant (Purdon and Weisskoff, 1998). Activated voxels were split into positive and negative groups. Positive BOLD responses exhibit a signal increase during annulus presentation, followed by a return to baseline, while negative BOLD responses exhibit a signal decrease during annulus presentation followed by a return to baseline (Cox et al., 1993; Haxby et al., 1994; Lee et al., 1995; Moskalenko et al., 1996; Saad et al., 2001; Seitz and Roland, 1992; Shulman et al., 1997a, 1997b; Woolsey et al., 1996). The choice of the cross correlation coefficient threshold determines the probability of falsely classifying an inactive voxel as active (type I error). However, by setting stringent thresholds, an increased number of active voxels are improperly classified as inactive (type II error). The presence of noise renders voxels showing stimulus-correlated response with low SNR indiscernible from those containing noise only. However, assuming noise is uncorrelated with the stimulus, one can increase the SNR of activated voxels to detectable levels by averaging multiple scans. With enough averaging, voxels containing noise only can be fully separated from those containing signal and noise without an increase in the type I error. To this end, we repeated the scans N_{rep} times ($5 < N_{\text{rep}} < 22$) and calculated average scans using N_{avg} scan repetitions, where N_{avg} was progressively varied between 2 and N_{rep} . To minimize any bias in the estimate of the average scan due to the order of scan acquisition, we used multiple scan permutations (up to 10, whenever possible) at each scan averaging level. The per-

mutations were determined using a random number generator. For example, for an averaging level of three ($N_{\text{avg}} = 3$), two permutations would be the average of scans 3, 7, and 18 and scans 2, 4, and 11, respectively. At each N_{avg} level, the mean volume (V_m) was estimated from the activation volumes at different permutations. We then modeled V_m as a function of N_{avg} using a logarithmic function of the form

$$V_m(N_{\text{avg}}) = V_m(1 + a \log(N_{\text{avg}})), \quad (1)$$

where V_m is the model estimate of V_m ; $V_m(1)$ is the mean activation volume at $N_{\text{avg}} = 1$, and a was determined using the Nelder–Mead simplex method implemented in Matlab (1994). The goodness of fit was assessed using the cross correlation coefficient between V_m and V_m .

Comparison of low- versus high-SNR responses

A hypothesis for the provenance of voxels with low SNR would be that extremely small responses occur in veins farther downstream from site of activation. In these distant veins, the hemodynamic changes are diluted due to mixing with blood from inactivated areas. As a consequence, detecting voxels with low SNR would worsen the localization of brain activation. It has been shown using independent methods that the delay of the BOLD response to stimulation is on average 0.7 to 2.4 s longer in distant vessels than in proximal ones (Kruggel and von Cramon, 1999a, 1999b; Saad et al., 2001). Thus if low-SNR voxels originate in distal veins, their response delays should be longer than those of proximal ones.

To test this hypothesis, we separated the set of activated voxels into low- and high-SNR pools and compared their response delay distributions. A low voxel is defined as a voxel that is detected as activated using N_{low} averaged scans or less. Conversely, a high voxel is defined as one detected as activated using only N_{high} averaged scans or more. Because N_{low} and N_{high} are arbitrary settings that can vary between 1 and N_{reps} , we performed comparisons between the two voxel pools at various combinations of N_{low} and N_{high} settings. This type of analysis can reveal significant trends in the data that may otherwise not be significant at any one level of threshold setting (Saad et al., 2001). A Student T test was used to determine the significance of the mean delay difference between the two pools. The SNR of activated voxels was approximated as the ratio of power at stimulus fundamental frequency over the remaining power in the signal. The error involved in estimating signal power from the fundamental frequency component is minimal since for the stimuli used in our data, the average FMRI response is correlated with a sinusoid to a level of 0.93 (Saad et al., 2001).

We also repeated the comparisons, excluding voxels that exhibit large percentages of signal change. Such voxels are likely to originate in larger proximal veins but have a short response delay relative to the capillary veins and venules. By excluding them from the delay distributions, we can

better detect delay differences, if any, between localized venous capillary signals and distal draining veins. The analysis was performed at percentage signal threshold levels of 3, 3.5, and 4%.

Simulated data

To further understand the expression of type I and type II errors with averaging, we created simulated FMRI data using two pools of time series, noise only (noise) and noise plus signal (activated). The union of these two pools represented a simulated FMRI data set. The main obstacles in creating simulated FMRI data lie in the nature of FMRI noise and the SNR distribution of the activated voxels. In the scope of this paper, we assume that FMRI noise is Gaussian and uncorrelated, temporally and spatially, and focus on the SNR distribution since it is of direct relevance to type II error estimates. The true SNR of activated voxels cannot be determined from empirical data because of the overlap between noise and signal spectra and the absence of an independent estimate of the noise power at stimulus frequency.

To create the simulated data, we estimated the fraction of activated voxels and their SNR distribution from empirical data. Using the average of 22 data sets, we detected activated voxels at a type I error probability of $P < 0.0001$ (Bonferroni corrected). We found that approximately 4% (1067 voxels) of the entire data set were activated. We then estimated the SNR of these same voxels in each of the 22 single-scan repetitions. The union of these 22 SNR distributions was used as an estimate of the SNR distribution of the detected activated FMRI voxels. A lognormal function was used to model this distribution and generate the SNR distribution of the simulated activated FMRI time series. The simulated time series data sets were averaged and the active voxels detected in similar fashion to the empirical data.

Results

Spatial extent of activation

Figure 1A shows the volume of activation (V_a) versus the averaging level N_{avg} for data obtained at 3 T using the small stimulus (2.2 to 3.6° eccentricity). Positive and negative BOLD volumes are marked by the ‘+’ and black dot symbols, respectively. At $N_{\text{avg}} = 1$, the symbols indicate the results from each of the 22 scan repetitions. At the remaining averaging levels, the symbols indicate the results from the various averaging permutations considered. The solid lines represent the fit of the mean volume (circles and triangles) V_m versus N_{avg} using the logarithmic function in Eq. 1. For positive and negative BOLD responses, the correlation coefficients between the logarithmic functions and the mean volumes were 0.99 and 0.96, respectively.

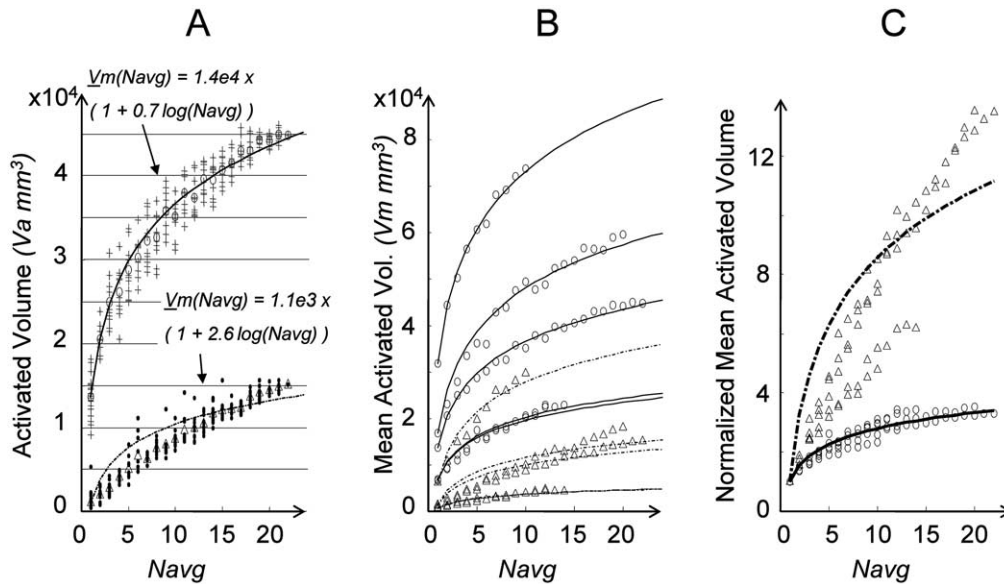


Fig. 1. (A) Volume of activation (V_a) versus averaging level N_{avg} for the small stimulus (2.2 to 3.6° eccentricity). Positive and negative BOLD volumes are marked by the plus symbols and black dot symbols, respectively. At $N_{avg} = 1$, the symbols indicate the results from each of the 22 scan repetitions. At the remaining averaging levels, the symbols indicate the results from the various averaging permutations considered. The solid lines represent the fit of the mean volume (circles and triangles) V_m versus N_{avg} using the logarithmic function in Eq. 1. (B) Mean volume of activation (V_m) versus averaging level N_{avg} for all data used in this study. The solid lines represent the fit of the average volume (circles and triangles) using the logarithmic function in Eq. 1. (C) Normalized mean volume of activation ($V_m/V_m(1)$) for the all empirical data shown in B. The lines represent the logarithmic fit of the average normalized volume versus averaging level for positive (circles) and negative (triangle) responses.

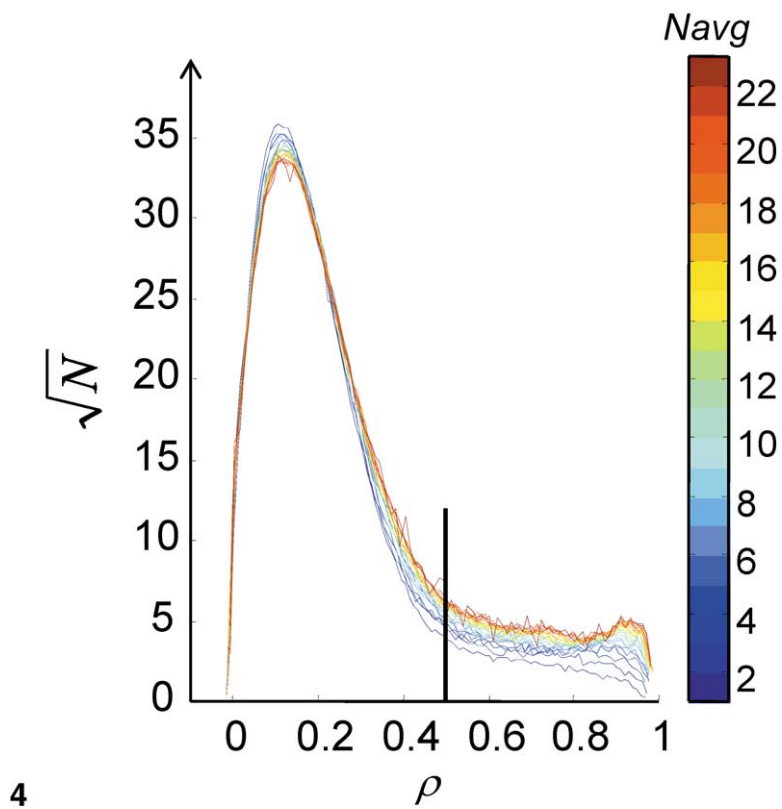
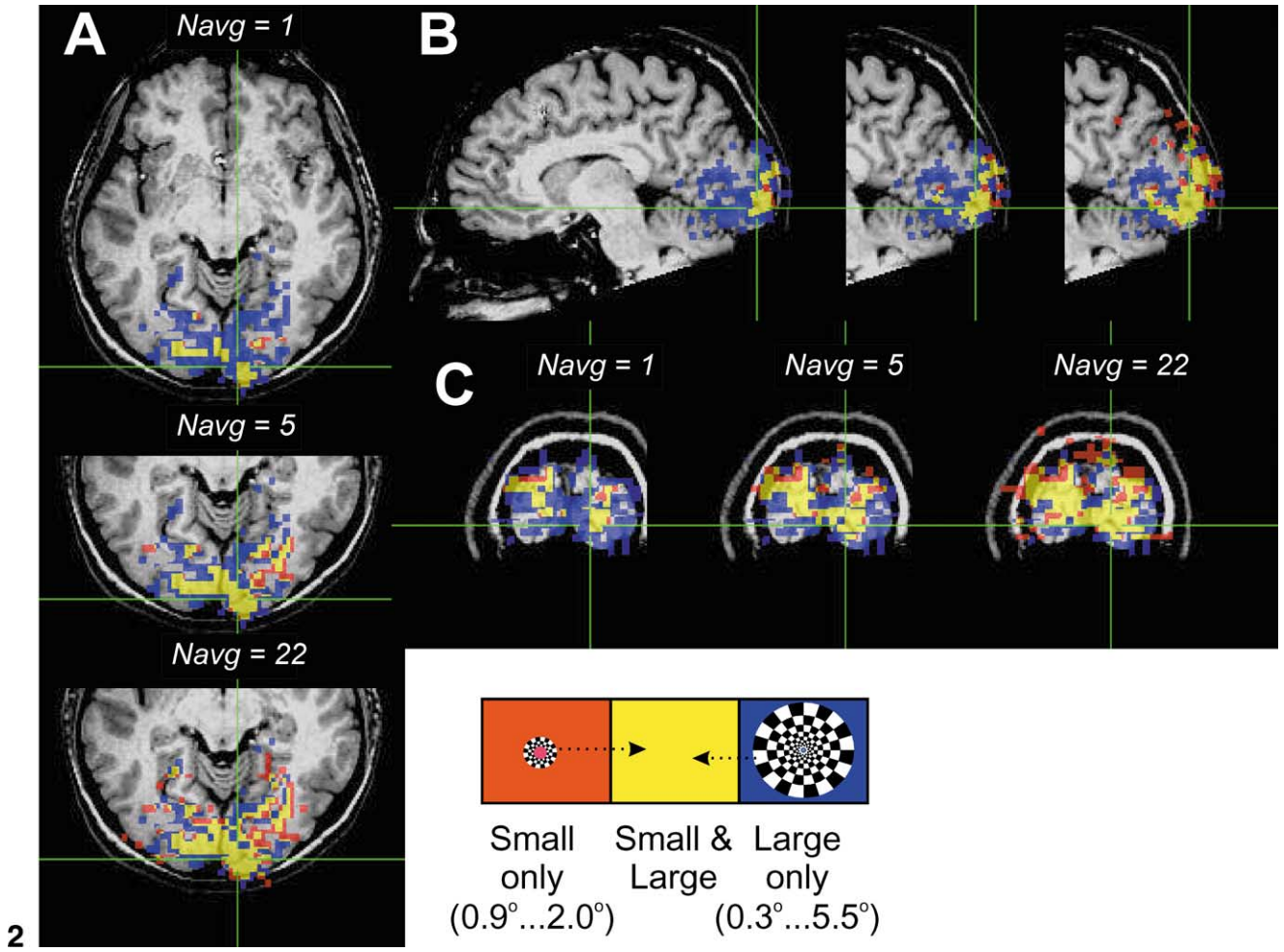
Note the monotonic increase in the activation volumes with increased averaging. For the positive BOLD response, increases of 50% of the initial volume occurred by averaging 2 scans, and increases of 100% occurred by averaging 4 or 5 scans. Increased averaging resulted in steady but smaller increases in activation volume with a factor of 3.3 increases at $N_{avg} = 22$. For the negative BOLD response, the increases in the volume of activation were more pronounced with averaging than those for the positive BOLD response. Activation volumes doubled by averaging 3 scans and continued increasing to achieve increases by a factor of 13 with 22 averaged scans. The ratio of positive to negative BOLD volume was 18.3 at $N_{avg} = 1$ and decreased to 3.0 at $N_{avg} = 22$. Note also that the activation volume was highly variable from scan to scan ($N_{avg} = 1$), with the largest positive volume (18225 mm³) being twice as large as the smallest one (9169 mm³). For negative responses, the scan to scan volume variability was more remarkable, with a ratio of 16 between the largest and smallest volumes. To determine whether systematic changes in noise or response

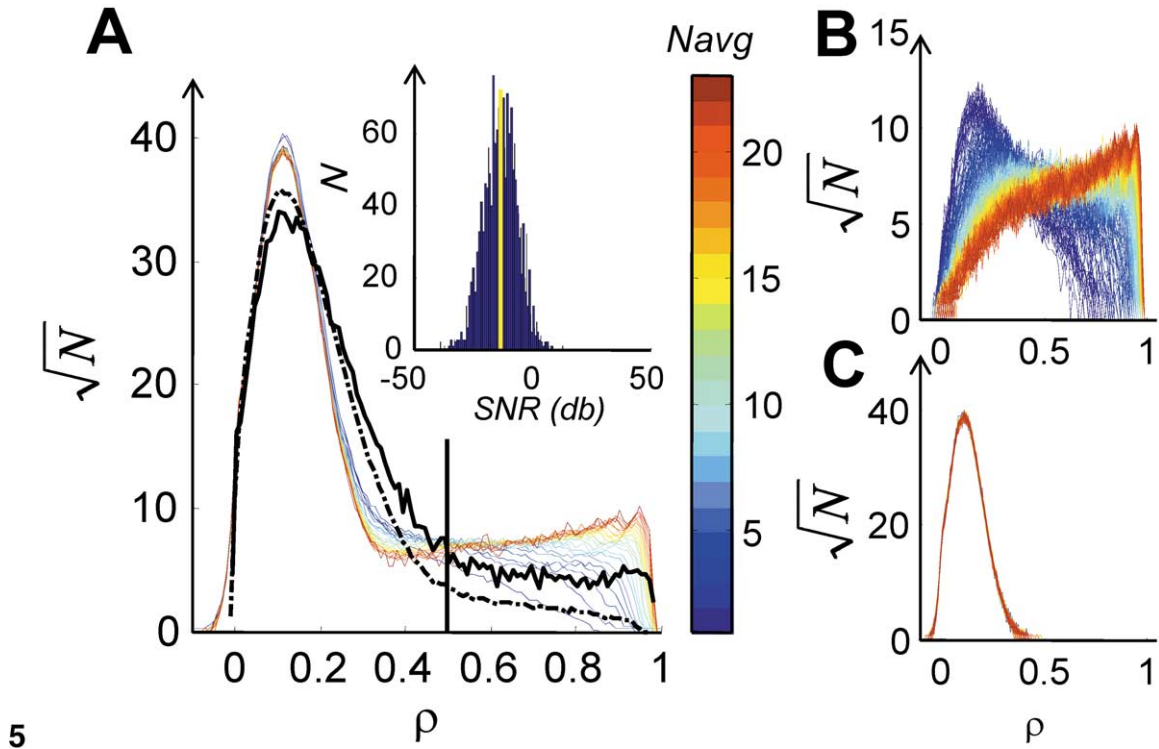
properties were causing the differences in activation volumes, we examined the signals in those voxels activated in all scan repetitions. We found no significant correlation ($P > 0.05$) between activation volume and SNR, signal, or noise power across repetitions. This suggests that changes in activation volumes at $N_{avg} = 1$ were not due to systemic changes in noise or signal power throughout the activated region.

Fig. 1B shows the combined results from all five data sets considered. For clarity, only the mean empirical volume (V_m) is shown at each averaging level. The solid and dash-dotted lines represent the curve fits to V_m according to Eq. 1. Values for a ranged between 0.56 and 0.89 for positive responses and 1.51 and 3.42 for negative responses. The trends were comparable across data sets despite differences in stimulus size and scanner field strengths and stimulus contrast. Fig. 1C shows V_m normalized by $V_m(1)$, the mean empirical volume at $N_{avg} = 1$. Solid and dash-dotted lines represent fits according to Eq. 1 to all positive ($a = 0.78$) and negative ($a = 3.28$) normalized volumes, respectively. Note the high correlation (0.99) for the positive responses

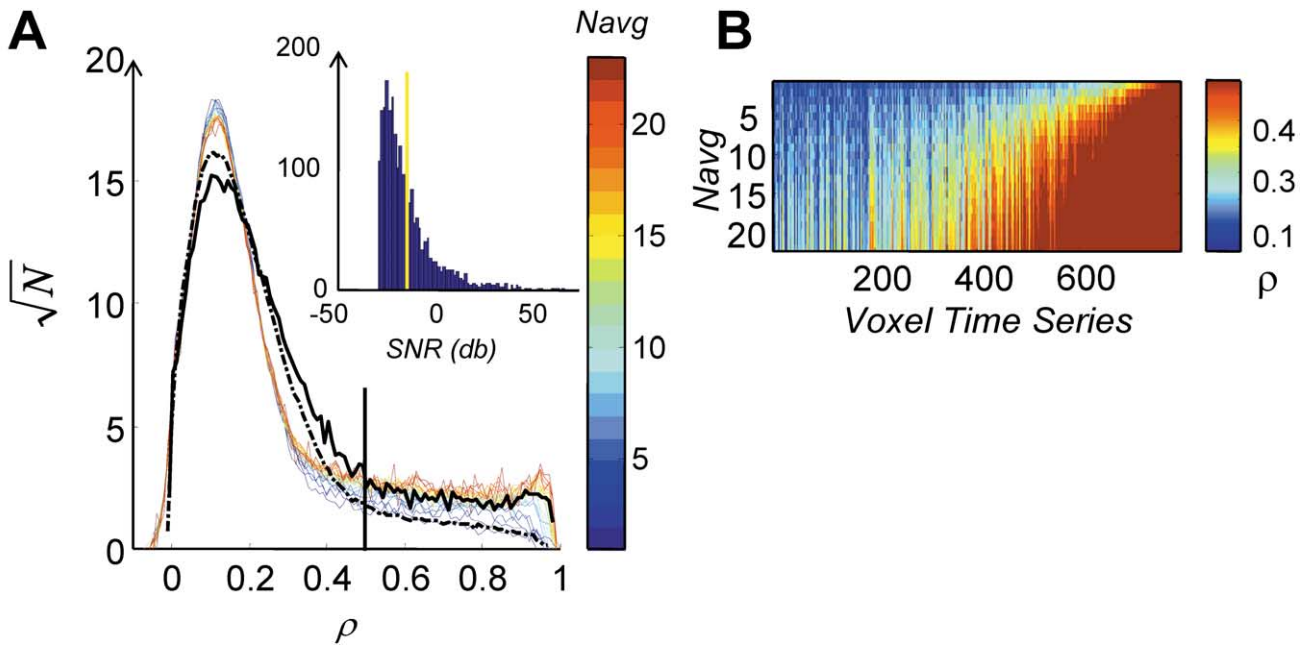
Fig. 2. Change in the spatial activation pattern with averaging in the axial (A), sagittal (B), and coronal (C) planes. Data from the small stimulus at N_{avg} of 1, 5, and 22 is overlaid on data from the large stimulus at $N_{avg} = 5$. Blue and red colors indicate voxels activated only by the large stimulus and only by the small stimulus, respectively. The yellow color indicates voxels activated by both small and large stimuli. Most of the activation induced by the small stimulus overlapped (yellow color) that of the large stimulus.

Fig. 4. Rootogram envelopes of the cross correlation coefficients (ρ) for different averaging levels, N_{avg} . The black vertical bar indicates the threshold used to classify voxels as activated ($P < 0.0001$). Different colors code for the averaging level at which the distribution was obtained. Note the decrease in the frequency of voxels with very low ρ (~ 0.15), with averaging thereby indicating the presence of numerous voxels that contain signal with very low SNR. With averaging, these voxels migrate toward higher ρ , which results in the observed decrease in frequency at ρ around 0.15.





5



6

Fig. 5. (A) Rootogram envelopes of simulated data using the SNR distribution derived from the empirical data. The PDF of this distribution, shown in the inset, was modeled as lognormal, with parameters $\mu = -3.1$ and $\sigma = 1.6$. The yellow line indicates the mean SNR. Different colors of the rootogram envelopes code for the averaging level N_{avg} used to obtain the distribution. The outermost envelopes from Fig. 4 ($N_{avg} = 1$ and $N_{avg} = 22$) are overlaid in black lines (dashed and solid, respectively) over the simulation rootogram. Note how, with increased averaging, the frequency decreased at ρ values between 0.2 and 0.5, and contrast this to the changes in the empirical histograms of Fig. 4. (B and C) Changes in the rootograms for the two simulated voxel populations, noise only and signal plus noise, are shown. Note the absence of variation in the noise-only rootograms, in sharp contrast to the signal plus noise rootograms.

Fig. 6. (A) Rootogram envelopes of simulated data using the lognormal ($\mu = 2.5$, $\sigma = 0.5$) SNR distribution shown in the inset. The outermost envelopes from Fig. 4 ($N_{avg} = 1$ and $N_{avg} = 22$) are overlaid in black lines (dashed and solid, respectively) over the simulation rootogram. Note the improved match in histogram trends between the simulation and the empirical data compared with Fig. 5. (B) Cross correlation coefficient versus averaging level for each voxel time series in the activated voxel pool. To preserve the dynamic range of the display, values larger than 0.5 were all colored dark red. Note the steady increase in ρ with averaging for all voxels, although many of these voxels do not reach the significance level without further averaging.

between the normalized volumes and their fit, despite the differences in the volume curves across subjects, scanner strengths, and stimulus size. For the negative responses, normalized volumes differed more markedly from the fit, although the correlation remained high at 0.96.

To test the sensitivity of the model in Eq. 1 to the number of data points used, we estimated the model parameters for the data in Fig. 1C using the first half of the data points only ($N_{\text{avg}} = 1 \dots 11$). With half of the volume estimates used, values for a were 0.74 and 2.5 for positive and negative responses, respectively. The model fit was correlated with the data at a level virtually identical to the one using all the data points. This indicated that the model was a good approximation of the data and not highly sensitive to the number of data samples.

At higher N_{avg} , the large increase in activation volume was centered about clusters originating during low N_{avg} . On average, a single cluster of contiguous voxels in the occipital cortex accounted for 90.5% of the activation volume. Fig. 2 shows the change in the spatial activation pattern with averaging in the axial, sagittal, and coronal planes. Data from the small stimulus at N_{avg} of 1, 5, and 22 are overlaid on data from the large stimulus at $N_{\text{avg}} = 5$. Blue and red colors indicate voxels activated only by the large stimulus and small stimulus, respectively. The yellow color indicates voxels activated by both small and large stimuli. Most of the activation induced by the small stimulus overlapped (yellow color) that of the large stimulus. Voxels activated by the small stimulus alone (red) were more numerous at high N_{avg} . However, they were mostly located on the periphery of the overlapping areas (yellow) rather than in isolated clusters. This suggests that some of the non-overlapping areas may be artifacts due to misalignment of EPI data collected on different sessions and aligned using the Talairach AC/PC landmarks: The data in Figs. 2 and 3 were obtained from subject S1 using the 3-T scanner. This data set was chosen because it contains the largest number of scans (22) and illustrates typical results from the remaining data sets. Note that Fig. 2 contains only positive BOLD responses. Negative BOLD responses occurred in clusters neighboring positive ones, as reported in Saad et al. (2001).

Comparison of low- versus high-SNR responses

Figure 3A shows an example of average time series from low- and high-SNR voxels at averaging levels of 1 (top) and 22 (bottom), respectively. In this example, low-SNR voxels were defined as those detected only after averaging 8 or more scans ($N_{\text{low}} = 8$) and high-SNR voxels were those detected by averaging at most 2 ($N_{\text{high}} = 2$) scans. The average percentages of signal change, measured at $N_{\text{avg}} = 22$, for the high- and low-SNR voxel pools were 1.98 and 0.66%, respectively. Note how the low-SNR time series appears to contain no significant signal component ($P > 0.0001$) at $N_{\text{avg}} = 1$. However, a clear signal component can be observed in the average time series from the same voxels obtained at $N_{\text{avg}} = 22$. Fig. 3B shows the

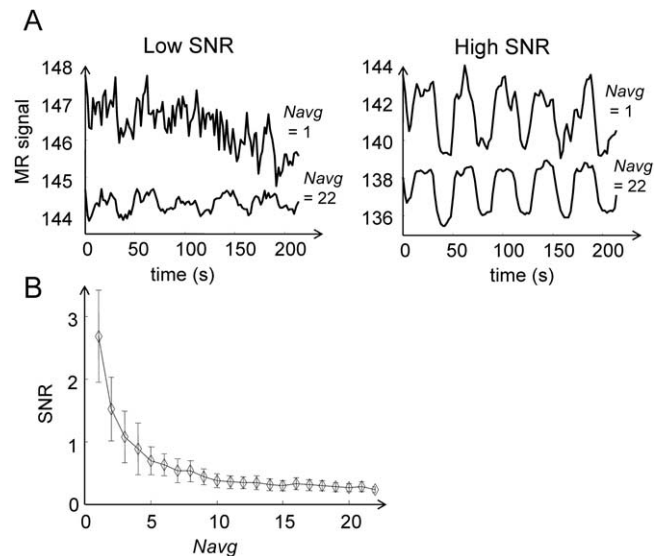


Fig. 3. (A) Average time series from low- and high-SNR voxels at averaging levels of 1 (top) and 22 (bottom), respectively. Low-SNR voxels were defined as those detected only after averaging 8 or more scans ($N_{\text{low}} = 8$) and high-SNR voxels were those detected by averaging at most 2 ($N_{\text{high}} = 2$) scans. Note how the low-SNR time series appear to contain no significant signal component ($P > 0.0001$) at $N_{\text{avg}} = 1$, although a clear signal component can be observed at $N_{\text{avg}} = 22$. (B) Correspondence between SNR and the averaging level required to detect an activated voxel. Diamonds represent the mean SNR of voxels detectable at different averaging levels, and the error bars extend 2 standard deviations.

correspondence between SNR and the averaging level required to detect an activated voxel. Diamonds represent the mean SNR of voxels detectable at different averaging levels and the error bars extend 2 standard deviations. The graph was compiled from all data sets presented in this study and is intended as a guide to the SNR level of a population of voxels detectable, in our data, at a particular averaging level. The data presented in this graph may not be applicable to time series with other noise and stimulus modulation frequency spectra. Noise spectra depend on a variety of factors, such as image sampling rate (TR), heart and respiration rates, and pulse sequence weighting.

To determine whether low-SNR responses originate in distal vasculature, we compared response delay differences between low- and high-SNR voxels across a range of N_{low} and N_{high} settings. We found no consistent and significant positive delay difference between high- and low-SNR voxels. In some instances, the difference in mean delay was significant ($P > 0.01$, Bonferroni corrected); however, it was not always positive and was not sustained across different values of N_{low} . In addition, no consistent delay difference was found when the analysis was repeated excluding voxels with larger percentages of signal change.

Cross correlation coefficient distributions

With increased averaging, voxels containing signal will exhibit an increase in the cross correlation coefficient (ρ , a

normalized measure of SNR), while those with no signal exhibit little change in either direction. Thus the ρ distribution of voxels containing signal will migrate to the right and further separate from the distribution of noise-only voxels. Fig. 4 shows the rootogram envelope of the cross correlation coefficients (ρ) for different averaging levels N_{avg} . The rootogram, which is the square root of the histogram, is used to enhance the changes in the tail of the distribution. The black bar indicates the threshold used to classify voxels as activated. The different colors code for the averaging level from which the distribution was obtained. The distribution at each N_{avg} is the average distribution across the various averaging permutations. With increasing N_{avg} , the frequency of voxels with higher ρ increased as expected. However, it is remarkable to note that the frequency of voxels with very low ρ (≈ 0.15) decreased. This indicates the presence of numerous voxels that contain signal with very low SNR. With averaging, these voxels migrate toward higher ρ , which results in the observed decrease in frequency at ρ around 0.15. However, even by averaging 22 scans, some of these activated voxels remain undetected, as evidenced by the distribution changes below the cross correlation threshold.

The shape and trends of the rootograms in Fig. 4 are governed by the percentage of activated voxels, their SNR distribution and the nature of fMRI noise. Since none of these parameters are known, we sought to reproduce the empirical distributions using simulated data sets. Fig. 5A shows the rootograms of the simulated data using the SNR distribution derived from the empirical data. The probability density function (PDF) of this distribution, shown in the inset, was modeled as lognormal with parameters $\mu = -3.1$ and $\sigma = 1.6$ (Hogg and Ledolter, 1987). The outermost envelopes from Fig. 4 ($N_{\text{avg}} = 1$ and $N_{\text{avg}} = 22$) are overlaid in black (dashed and solid, respectively) over the simulation rootogram in order to highlight the differences between the simulated distributions and the empirical ones. In this simulation, 15% of the voxels contained signal. The choice of 15% signal ratio was arbitrary, with the only condition being that it is higher than 4%, the fraction of voxels detected as activated at $N_{\text{avg}} = 22$. Increasing the percentage of voxels with signal has the effect of enhancing the trends observed at all sections of the rootogram and a rise in the right side of the main lobe. Note how, with increased averaging, the frequency decreased at ρ values between 0.2 and 0.5. This is in contrast to the empirical histograms of Fig. 4, where increases in the distribution were observed at ρ close to 0.15. Figs. 5B and C show the changes in the rootograms for the two stimulated voxel populations, noise only and signal plus noise. Note the absence of variation in the noise-only rootograms in sharp contrast to the signal plus noise distribution.

To better match the rootograms observed in empirical data, we repeated the simulations using other lognormal noise distributions. Fig. 6A shows the results obtained using a lognormal ($\mu = 2.5$, $\sigma = 0.5$) SNR distribution shown in

the inset. Compared with the empirical SNR distribution, the lognormal distribution used here contains a higher density of voxels with low SNR. This resulted in increases in ρ distribution occurring at ρ close to 0.2. Note how, in general, the trends in the rootogram changes are similar between the simulation and the empirical data. However, there is a notable mismatch between the magnitude of the peak and the width of the main lobe. Increasing the percentage of voxels with signal would reduce this discrepancy; however, the mismatch becomes very large at the tail of the histogram. Fig. 6B shows the increase in ρ with averaging for activated voxels in the simulated data set. Note how ρ increases for all the voxels but fails to reach significance for voxels with low SNR.

Task performance

Subject performance on the visual task for the data collected at 3T showed no consistent or significant differences in performance between the ON and OFF periods. On average, subject performance was 78% during the ON period and 80% during the OFF period, with no significant difference ($P > 0.01$) between the two states. When two of the three subjects performed the off-fixation task, their performance decreased significantly ($P < 0.01$) from 87 to 67% for S1 and from 91 to 71% for S3. They reported that the off-fixation task was more difficult and required a conscious suppression of an urge to saccade back to the central fixation point. Task performance was not significantly correlated ($P > 0.01$) with the time of scan acquisition during the experiment or with the volume of activation.

Discussion

The volume of activation was found to increase considerably with averaging for both positive and negative BOLD responses. This result indicates that the extent of the BOLD response is much larger than previously conjectured. Recently, Huettel and McCarthy (2001) also reported increasing activation volumes with increasing numbers of evoked responses to brief visual stimuli. However, the volume increases observed in our study are more substantial since the stimulus and its time course were designed to induce strong modulation in the BOLD signal. The function we used to model the volume of activation as a function of the number of averaged scans was chosen because of its asymptotic nature and accuracy even when half of the data points were used. For positive responses, normalized activation volume curves were remarkably constant across subject, scanner field strengths, stimulus size, and contrast. This suggests that the log model may be used to estimate the volume of activation beyond the range of empirical data. For the negative responses, there was more variability in normalized activation volume curves and the model fit may be inadequate for extrapolation. The activation volume curves indi-

cate that for positive BOLD responses, most of the volume increase occurs at the average of 5 scans. However, while the volume increases grew smaller with further averaging, they did not plateau, and the average volume at 22 averaged scans was 50% larger than that at 5 averaged scans. For the negative responses, the trends were more pronounced, and the increases were still on the order of 40% of the initial volume at averaging levels of 20. The differences between the positive and negative response curves are likely due to the weaker SNR of the latter.

The observation that volume curves do not plateau suggests that activated voxels remain undetected because of their low SNR. The presence of such voxels can be visualized by monitoring the trends in the rootograms with averaging. Those trends indicate that there is a considerable number of voxels activated with very low SNR that remain undetected as type II errors even with considerable scan averaging because their SNR fails to reach the threshold criterion at the preset type I error level. However, it may be possible to predict the total number of voxels that are type II errors by monitoring the progression of the SNR (or ρ) with increased averaging and comparing it with the progression with time series containing noise only.

The simulations illustrated how different SNR distributions in activated voxels affect the patterns of variation of the cross correlation coefficient rootograms with averaging. For normally distributed noise, the noise ρ distribution remained constant with averaging. This was expected since the number of degrees of freedom remained the same with averaging. Thus changes in the population rootograms were solely due to changes in the rootograms of voxels containing signal. By using the signal SNR distribution derived from empirical data, we found that the simulation rootograms differed markedly from the empirical rootograms. The differences were manifested at the peak and right side of the main lobe and the tail of the distributions. This suggested that matching the empirical histograms required a larger proportion of voxels with low SNR. The lognormal distribution accomplished this match and resulted in pattern changes that were comparable to those of the empirical data. However, some differences remained, mainly in the height of the peak and the width of the main lobe. These differences were likely due to the differences between FMRI noise and the Gaussian noise used in the simulation. The use of FMRI noise, which is spatially correlated, may result in a wider main lobe and, consequently, a lower peak. A detailed analysis of these issues is beyond the scope of this paper and requires collecting a large set of FMRI data that contains noise only. This can be achieved by using a stimulus containing the fixation task alone, without the annulus (no cyclic stimulation).

There was also considerable change in the volume of activation from one scan to the next (at $N_{\text{avg}} = 1$). Activation volumes were not correlated with task performance or the sequence of scan acquisition, which suggests that volume changes do not reflect changes in attention levels,

habituation, or learning. These results complement those reported by Noll et al. (1997) and McGonigle et al. (2000), who observed significant variation in the activation volume of scans obtained from the same subject over periods as short as a scanning session and as long as 2 months. Furthermore, activation volumes were not significantly correlated with SNR, signal, or noise power of voxels activated at all scan repetitions. Thus volume changes do not appear to result from systemic changes in signal or noise levels. However, it is possible that subtle variations in the noise spectrum can result in large changes in activation volumes. For example, changes in the phase difference between the same signal and noise frequencies could have additive or subtractive effects on the SNR and, consequently, on the activation volume across scans (Saad, 1996). These subtle effects are amplified by the presence of a large proportion of voxels with low SNR and the nonrandom nature of FMRI noise components, such as heart rate, respiration, and physiological fluctuations (Biswal et al., 1996; Buonocore and Maddock, 1997). The effects of voxels with low SNR on the activation volume are also obvious when analyzing the change in activation volume versus cross correlation coefficient threshold ρ_t . A change in ρ_t from 0.55 to 0.45 would result in a twofold increase in the activation volume. Whatever the causes of variability, the use of activation volumes as a metric for assessing functional activation can yield erroneous conclusions even if an effort is made to equalize task performance across scans. For volume-based longitudinal studies, it is critical to also assess the variance of the activation volume for each effect considered.

The spatial expansion of the activated volume with averaging was not random and was centered on clusters activated in single scans. However, the increases were not omnidirectional and, for a small stimulus with higher averaging, followed the patterns generated by a stimulus of a larger size. In addition, volume increases are not likely an artifact of the stimulus properties, imaging point spread function, or venous drainage. The stimulus was designed to produce photic stimulation in a restricted region of the visual field and modulate mostly low-level visual areas. Care was taken to make the stimulus equiluminant and minimize reflected flicker to imperceptible levels. Furthermore, the stimulus and task were designed to help maintain attention and fixation on the fixation square in the center of the stimulus. Imaging point spread function artifacts, which are caused by the sampling process and spin relaxation rates (Farzaneh et al., 1990), occur in the imaging plane (axial) in both phase and frequency encoding directions and manifest themselves outside the brain, where thermal noise is considerably less than physiological noise. Furthermore, point spread artifacts do not explain the overlap between the asymmetric response pattern of larger stimulus and that of the small response with high averaging, as illustrated in Fig. 2A. The increases are also not a likely artifact of distal venous drainage. Voxels mapped to distal blood vessels have been shown to have, on average, a response delay

difference of 1 or 2 s relative to voxels mapped to proximal ones (Krugger and von Cramon, 1999b; Saad et al., 2001). Here, we found no evidence for consistent response delay differences between low- and high-SNR voxels despite the analysis technique, which has been shown to reveal small but consistent delay differences between the two voxel pools (Saad et al., 2001).

The large extent of BOLD activation may simply be caused by a large spread of the hemodynamic response to localized activation, with the largest increases closest to the site of activation and decreasing responses farther away, or by dephasing effects from weak gradients in a distal network of large venous vessels. The latter hypothesis can be tested using spin-echo sequences, which are insensitive to these spatially extensive gradients. Alternately, however, the extent of activation may occur in response to local field potential (LFP) changes caused by the subthreshold activity of long-range horizontal connections (Das and Gilbert, 1995; Gilbert et al., 1996; Grinvald et al., 1994; Takashima et al., 2001). Using optical imaging techniques and extracellular electrodes, Das and Gilbert (1995) have shown that neural spiking accounted for 5% of the activated area detected with optical dyes, with the remaining 95% due to subthreshold activity. Recently, Logothetis et al. (2001) presented direct evidence suggesting that BOLD signals correlate more with LFP than with neuronal spiking alone.

Conclusions

Using visual stimulation in a restricted region of the visual field and a large number of scan repetitions, we found large increases in the volume of BOLD response with averaging. A large proportion of activated voxels has low SNR and remains undetected without considerable averaging. We found up to a twofold increase in the volume of activated voxels across scans. This volume change was not correlated with the order of acquisition or subject performance on the visual task, nor was it correlated with systemic changes in noise or signal properties. However, given the large proportion of voxels with low SNR and the nature of fMRI noise, subtle changes between overlapping noise and signal frequency components can account for the volume differences. Even with extensive averaging, many activated voxels remained undetected because of their low SNR. The existence of such voxels was revealed by changes in the cross correlation coefficient distribution with increased averaging. The spatial increase in the extent of activated voxels was centered about loci of activation that appear with little or no scan averaging. The primary reason for this was not downstream venous drainage since there was no significant and consistent delay difference between voxels activated at different averaging levels. The increased spatial extent may reflect a diffuse subthreshold activity centered about spiking neurons, weak dephasing gradients from distal venous ves-

sels, or simply a blood flow response extending beyond the locus of neuronal firing.

Acknowledgments

This research was supported by the intramural NIMH research program and by a Whitaker Foundation Special Opportunity Predoctoral fellowship (Z.S.), an Anthony J. and Rose Eanelli Bagozzi Medical Research Fellowship (K.M.R.), and NIH Grants EY10244, MH51358, and CRC1234 (E.A.D.).

References

- Arthurs, O.J., Williams, E.J., Carpenter, T.A., Pickard, J.D., Boniface, S.J., 2000. Linear coupling between functional magnetic resonance imaging and evoked potential amplitude in human somatosensory cortex. *Neuroscience* 101(4), 803–806.
- Bandettini, P.A., Ungerleider, L.G., 2001. From neuron to BOLD: new connections. *Nature Neurosci.* 4(9), 864–866.
- Bandettini, P.A., Wong, E.C., 1997. A hypercapnia-based normalization method for improved spatial localization of human brain activation with fMRI. *NMR Biomed.* 10(4–5), 197–203.
- Bandettini, P.A., Wong, E.C., Hinks, R.S., Tikofsky, R.S., Hyde, J.S., 1992. Time course EPI of human brain function during task activation. *Magn. Reson. Med.* 25, 390–397.
- Beauchamp, M.S., Cox, R.W., DeYoe, E.A., 1997. Graded effects of spatial and featural attention on human area MT and associated motion processing areas. *J. Neurophysiol.* 78(1), 516–520.
- Birn, R.M., Saad, Z.S., Bandettini, P.A., 2001. Spatial heterogeneity of the nonlinear dynamics in the fmri bold response. *Neuroimage* 14(4), 817–826.
- Biswal, B., DeYoe, E.A., Hyde, J.S., 1996. Reduction of physiological fluctuations in FMRI using digital filters. *Magn. Reson. Med.* 35, 107–113.
- Boynton, G., Engel, S., Glover, G., Heeger, D., 1996. Linear systems analysis of functional magnetic resonance imaging in human V1. *J. Neurosci.* 16(13), 4207–4221.
- Brefczynski, J.A., DeYoe, E.A., 1999. A physical correlate of the ‘spotlight’ of visual attention. *Nature Neurosci.* 2(4), 370–374.
- Buonocore, M.H., Maddock, R.J., 1997. Noise suppression digital filter for functional magnetic resonance imaging based on image reference data. *Magn. Reson. Med.* 38(3), 456–469.
- Buxton, R.B., 2001. The elusive initial dip. *Neuroimage* 13(6 Pt. 1), 953–958.
- Buxton, R.B., Wong, E.C., Frank, L.R., 1998. Dynamics of blood flow and oxygenation changes during brain activation: the balloon model. *Magn. Reson. Med.* 39(6), 855–864.
- Cohen, M.S., 1997. Parametric analysis of FMRI data using linear systems methods. *Neuroimage* 6, 93–103.
- Cox, R.W., Hyde, J.S., 1997. Software tools for analysis and visualization of fMRI data. *NMR Biomed.* 10(4–5), 171–178.
- Cox, S.B., Woolsey, T.A., Rovainen, C.M., 1993. Localized dynamic changes in cortical blood flow with whisker stimulation corresponds to matched vascular and neuronal architecture of rat barrels. *J. Cereb. Blood Flow Metab.* 13(6), 899–913.
- Das, A., Gilbert, C.D., 1995. Long-range horizontal connections and their role in cortical reorganization revealed by optical recording of cat primary visual cortex. *Nature* 375(6534), 780–784.
- Davis, T., Kwong, K., Weisskoff, R., Rosen, B., 1998. Calibrated functional MRI: mapping the dynamics of oxidative metabolism. *Proc. Natl. Acad. Sci. USA* 95(4), 1834–1839.

- DeYoe, E.A., Bandettini, P., Neitz, J., Miller, D., Winans, P., 1994. Functional magnetic resonance imaging (fMRI) of the human brain. *J. Neurosci. Methods* 54, 171–187.
- DeYoe, E.A., Van Essen, D.C., 1988. Concurrent processing streams in monkey visual cortex. *Trends Neurosci.* 11(5), 219–226.
- Duong, T.Q., Kim, D.S., Ugurbil, K., Kim, S.G., 2000. Spatiotemporal dynamics of the BOLD fMRI signals: toward mapping submillimeter cortical columns using the early negative response. *Magn. Reson. Med.* 44(2), 231–242.
- Duong, T.Q., Kim, D.S., Ugurbil, K., Kim, S.G., 2001. Localized cerebral blood flow response at submillimeter columnar resolution. *Proc. Natl. Acad. Sci. USA* 28, 28.
- Engel, S., Glover, G., Wandell, B., 1997. Retinotopic organization in human visual cortex and the spatial precision of functional MRI. *Cereb. Cortex* 7(2), 181–192.
- Farzaneh, F., Riederer, S.J., Pelc, N.J., 1990. Analysis of T2 limitations and off-resonance effects on spatial resolution and artifacts in echo-planar imaging. *Magn. Reson. Med.* 14(1), 123–139.
- Felleman, D.J., Van Essen, D.C., 1991. Distributed hierarchical processing in the primate cerebral cortex. *Cereb. Cortex* 1(1), 1–47.
- Friston, K.J., Josephs, O., Rees, G., Turner, R., 1998. Nonlinear event-related responses in fMRI. *Magn. Reson. Med.* 39, 41–52.
- Genovese, C.R., Noll, D.C., Eddy, W.F., 1997. Estimating test-retest reliability in functional MR imaging. I: Statistical methodology. *Magn. Reson. Med.* 38(3), 497–507.
- Gilbert, C.D., Das, A., Ito, M., Kapadia, M., Westheimer, G., 1996. Spatial integration and cortical dynamics. *Proc. Natl. Acad. Sci. USA* 93(2), 615–622.
- Goodyear, B.G., Menon, R.S., 2001. Brief visual stimulation allows mapping of ocular dominance in visual cortex using fMRI. *Hum. Brain Mapp.* 14(4), 210–217.
- Grinvald, A., Lieke, E.E., Frostig, R.D., Hildesheim, R., 1994. Cortical point-spread function and long-range lateral interactions revealed by real-time optical imaging of macaque monkey primary visual cortex. *J. Neurosci.* 14(5 Pt 1), 2545–2568.
- Haxby, J.V., Horwitz, B., Ungerleider, L.G., Maisog, J.M., Pietrini, P., Grady, C.L., 1994. The functional organization of human extrastriate cortex: a PET-rCBF study of selective attention to faces and locations. *J. Neurosci.* 14(11), 6336–6353.
- Hess, A., Stiller, D., Kaulisch, T., Heil, P., Scheich, H., 2000. New insights into the hemodynamic blood oxygenation level-dependent response through combination of functional magnetic resonance imaging and optical recording in gerbil barrel cortex. *J. Neurosci.* 20(9), 3328–3338.
- Hogg, R.V., Ledolter, J., 1987. *Engineering Statistics*. Macmillan, New York.
- Hoogenraad, F.G., Pouwels, P.J., Hofman, M.B., Reichenbach, J.R., Sprenger, M., Haacke, E.M., 2001. Quantitative differentiation between BOLD models in fMRI. *Magn. Reson. Med.* 45(2), 233–246.
- Horton, J.C., Hoyt, W.F., 1991. The representation of the visual field in human striate cortex. A revision of the classic Holmes map. *Arch. Ophthalmol.* 109(6), 816–824.
- Huettel, S.A., McCarthy, G., 2001. The effects of single-trial averaging upon the spatial extent of fMRI activation. *Neuroreport* 12(11), 2411–2416.
- Karni, A., Meyer, G., Jezzard, P., Adams, M.M., Turner, R., Ungerleider, L., 1995. Functional MRI evidence for adult motor cortex plasticity during motor skill learning. *Nature* 377, 155–158.
- Kastner, S., De Weerd, P., Desimone, R., Ungerleider, L., 1998. Mechanisms of directed attention in the human extrastriate cortex as revealed by functional MRI. *Science* 282(5386), 108–111.
- Kim, D.S., Duong, T.Q., Kim, S.G., 2000. High-resolution mapping of iso-orientation columns by fMRI. *Nature Neurosci.* 3(2), 164–169.
- Kim, S.G., Rostrup, E., Larsson, H.B., Ogawa, S., Paulson, O.B., 1999. Determination of relative CMRO₂ from CBF and BOLD changes: significant increase of oxygen consumption rate during visual stimulation. *Magn. Reson. Med.* 41(6), 1152–1161.
- Kim, S.G., Ugurbil, K., 1997. Comparison of blood oxygenation and cerebral blood flow effects in fMRI: estimation of relative oxygen consumption change. *Magn. Reson. Med.* 38(1), 59–65.
- Kinahan, P.E., Noll, D.C., 1999. A direct comparison between whole-brain PET and BOLD fMRI measurements of single-subject activation response. *Neuroimage* 9(4), 430–438.
- Krings, T., Reinges, M.H., Erberich, S., Kemeny, S., Rohde, V., Spetzger, U., Korinth, M., Willmes, K., Gilsbach, J.M., Thron, A., 2001. Functional MRI for presurgical planning: problems, artefacts, and solution strategies. *J. Neurol. Neurosurg. Psychiatry* 70(6), 749–760.
- Kruggel, F., von Cramon, D.Y., 1999a. Modeling the hemodynamic response in single-trial functional MRI experiments. *Magn. Reson. Med.* 42(4), 787–797.
- Kruggel, F., von Cramon, D.Y., 1999b. Temporal properties of the hemodynamic response in functional MRI. *Hum. Brain Mapp.* 8(4), 259–271.
- Kwong, K.K., Belliveau, J.W., Chesler, D.A., Goldberg, I.E., Weisskoff, R.M., Poncelet, B.P., Kennedy, D.N., Hoppel, B.E., Cohen, M.S., Turner, R., 1992. Dynamic magnetic resonance imaging of human brain activity during primary sensory stimulation. *Proc. Natl. Acad. Sci. USA* 89(12), 5675–5679.
- Lai S, Hopkins, AL, Haacke, EM, Li D, Wasserman BA, Buckley P, Friedman L, Meltzer H, Hedera P, R. F. 1993. Identification of vascular structure as a major source of signal contrast in high resolution 2D and 3D functional activation imaging of the motor cortex at 1.5T: Preliminary results. *Magn. Reson. Med.* (30), 387–392.
- Lee, A.T., Glover, G.H., Meyer, C.H., 1995. Discrimination of large venous vessels in time-course spiral blood-oxygen-level-dependent magnetic-resonance functional neuroimaging. *Magn. Reson. Med.* (33), 745–754.
- Liu, H., Gao, J., 2000. An investigation of the impulse functions for the nonlinear BOLD response in functional MRI. *Magn. Reson. Imaging* 18(8), 931–938.
- Liu, Y., Pu, Y., Fox, P.T., Gao, J.H., 1999. Quantification of dynamic changes in cerebral venous oxygenation with MR phase imaging at 1.9 T. *Magn. Reson. Med.* 41(2), 407–411.
- Logothetis, N.K., Pauls, J., Augath, M., Trinath, T., Oeltermann, A., 2001. Neurophysiological investigation of the basis of the fMRI signal. *Nature* 412(6843), 150–157.
- Magistretti, P.J., 2000. Cellular bases of functional brain imaging: insights from neuron-glia metabolic coupling. *Brain Res.* 886(1–2), 108–112.
- Magistretti, P.J., Pellerin, L., Rothman, D.L., Shulman, R.G., 1999. Energy on demand. *Science* 283(5401), 496–497.
- Mandeville, J.B., Marota, J.J., Kosofsky, B.E., Keltner, J.R., Weissleder, R., Rosen, B.R., Weisskoff, R.M., 1998. Dynamic functional imaging of relative cerebral blood volume during rat forepaw stimulation. *Magn. Reson. Med.* 39(4), 615–624.
- Mandeville, J.B., Marota, J.J.A., Ayata, C., Moskowitz, M.A., Weisskoff, R.M., Rosen, B.R., 1999. MRI Measurement of the temporal evolution of relative CMRO₂ during rat forepaw stimulation. *Magn. Reson. Med.* 42, 944–951.
- Manoach, D.S., Halpern, E.F., Kramer, T.S., Chang, Y., Goff, D.C., Rauch, S.L., Kennedy, D.N., Gollub, R.L., 2001. Test-retest reliability of a functional MRI working memory paradigm in normal and schizophrenic subjects. *Am. J. Psychiatry* 158(6), 955–958.
- Marota, J.J., Ayata, C., Moskowitz, M.A., Weisskoff, R.M., Rosen, B.R., Mandeville, J.B., 1999. Investigation of the early response to rat forepaw stimulation. *Magn. Reson. Med.* 41(2), 247–252.
- Matlab, V., 1994. *Signal Processing Toolbox User's Guide*. The Math Works, Natick, MA.
- McGonigle, D.J., Howseman, A.M., Athwal, B.S., Friston, K.J., Frackowiak, R.S., Holmes, A.P., 2000. Variability in fMRI: an examination of intersession differences. *Neuroimage* 11(6 Pt 1), 708–734.
- Menon, R.S., Goodyear, B.G., 1999. Submillimeter functional localization in human striate cortex using BOLD contrast at 4 Tesla: implications for the vascular point-spread function. *Magn. Reson. Med.* 41(2), 230–235.

- Menon, R.S., Ogawa, S., Tank, D.W., Ugurbil, K., 1993. 4 Tesla gradient recalled echo characteristics of photic stimulation induced signal changes in the human primary visual cortex. *Magn. Reson. Med.* 30, 380–386.
- Miller, K.L., Luh, W.M., Liu, T.T., Martinez, A., Obata, T., Wong, E.C., Frank, L.R., Buxton, R.B., 2001. Nonlinear temporal dynamics of the cerebral blood flow response. *Hum. Brain Mapp.* 13(1), 1–12.
- Moskalenko, Y., Dowling, J., Liu, D., Rovainen, C., Semernia, V., 1996. LCBF changes in rat somatosensory cortex during whisker stimulation monitored by dynamic H₂ clearance. *Int. J. Psychophysiol.* 21(1), 45–59.
- Noll, D.C., Genovese, C.R., Nystrom, L.E., Vazquez, A.L., Forman, S.D., Eddy, W.F., Cohen, J.D., 1997. Estimating test-retest reliability in functional MR imaging. II: Application to motor and cognitive activation studies. *Magn. Reson. Med.* 38(3), 508–517.
- Ogawa, S., Lee, T., Nayak, S., Glynn, P., 1990a. Oxygenation-sensitive contrast in magnetic resonance image of rodent brain in high magnetic fields. *Magn. Reson. Med.* 14, 68–78.
- Ogawa, S., Lee, T.M., 1992. Blood oxygenation level dependent MRI of the brain: effects of seizure induced by kainic acid in rat. *Proc. Soc. Magn. Reson. Med.* 1, 501.
- Ogawa, S., Lee, T.M., Kay, A.R., Tank, D.W., 1990b. Brain magnetic resonance imaging with contrast dependent on blood oxygenation. *Proc. Natl. Acad. Sci. USA* 87, 9868–9872.
- Purdon, P.L., Weisskoff, R.M., 1998. Effect of temporal autocorrelation due to physiological noise and stimulus paradigm on voxel-level false-positive rates in fMRI. *Hum. Brain Mapp.* 6(4), 239–249.
- Rombouts, S.A., Barkhof, F., Hoogenraad, F.G., Sprenger, M., Valk, J., Scheltens, P., 1997. Test-retest analysis with functional MR of the activated area in the human visual cortex. *AJNR Am. J. Neuroradiol.* 18(7), 1317–1322.
- Saad, Z.S., 1996. Functional magnetic resonance imaging: activated time course detection and phase analysis, in: *Biomedical Engineering*, Marquette University, Milwaukee, p. 110.
- Saad, Z.S., DeYoe, E.A., Ropella, K.M., 2002. Estimation of fMRI response delays. *Neuroimage* 18(2), 494–508.
- Saad, Z.S., Ropella, K.M., Cox, R.W., DeYoe, E.A., 2001. Analysis and use of fMRI response delays. *Hum. Brain Mapp.* 13(2), 74–93.
- Savoy, R.L., 2001. History and future directions of human brain mapping and functional neuroimaging. *Acta Psychol.* 107(1–3), 9–42.
- Segebarth, C., Belle, V., Delon, C., Massoselli, R., Decety, G., LeBas, G.F., Decorps, M., Benabid, L.A., 1994. Functional MRI of the human brain: predominance of signals from extracerebral veins. *Neuroreport* 5, 813–816.
- Seitz, R.J., Roland, P.E., 1992. Vibratory stimulation increases and decreases the regional cerebral blood flow and oxidative metabolism: a positron emission tomography (PET) study. *Acta Neurol. Scand.* 86(1), 60–67.
- Shulman, G.L., Corbetta, M., Buckner, R.L., Fiez, J.A., Miezin, F.M., Raichle, M.E., Petersen, aS.E., 1997a. Common blood flow changes across visual tasks: I. Increases in subcortical structures and cerebellum but not in nonvisual cortex. *J. Cogn. Neurosci.* 9(5), 624–663.
- Shulman, G.L., Fiez, J.A., Corbetta, M., Buckner, R.L., Miezin, F.M., Raichle, M.E., Petersen, aS.E., 1997b. Common blood flow changes across visual tasks: II. Decreases in cerebral cortex. *J. Cogn. Neurosci.* 9(5), 648–663.
- Somers, D., Dale, A., Seiffert, A., Tootell, R., 1999. Functional MRI reveals spatially specific attentional modulation in human primary visual cortex. *Proc. Natl. Acad. Sci. USA* 96(4), 1663–1668.
- Takashima, I., Kajiwara, R., Iijima, T., 2001. Voltage-sensitive dye versus intrinsic signal optical imaging: comparison of optically determined functional maps from rat barrel cortex. *Neuroreport* 12(13), 2889–2894.
- Talairach, J., Tournoux, P., 1988. *Co-planar Stereotaxic Atlas of the Human Brain: An Approach to Medical Cerebral Imaging*. Thieme, Stuttgart.
- Tootell, R., Hadjikhani, N., Hall, E., Marrett, S., Vanduffel, W., Vaughan, J., Dale, A., 1998. The retinotopy of visual spatial attention. *Neuron* 21(6), 1409–1422.
- Vasquez, L.A., Noll, D.C., 1998. Nonlinear aspects of the BOLD response in functional MRI. *Neuroimage* 7, 108–118.
- Villringer, A., 1997. Understanding functional neuroimaging methods based on neurovascular coupling. *Adv. Exp. Med. Biol.* 413, 177–193.
- Villringer, A., Dirnagl, U., 1995. Coupling of brain activity and cerebral blood flow: basis of functional neuroimaging. *Cerebrovasc. Brain Metab. Rev.* 7(3), 240–276.
- Woolsey, T., Rovainen, C., Cox, S., Henegar, M., Liang, G., Liu, D., Moskalenko, Y., Sui, J., Wei, L., 1996. Neuronal units linked to microvascular modules in cerebral cortex: response elements for imaging the brain. *Cereb. Cortex.* 6(5), 647–660.
- Yacoub, E., Le, T.H., Ugurbil, K., Hu, X., 1999. Further evaluation of the initial negative response in functional magnetic resonance imaging. *Magn. Reson. Med.* 41(3), 436–441.
- Yang, X., Hyder, F., Shulman, R.G., 1997. Functional MRI BOLD signal coincides with electrical activity in the rat whisker barrels. *Magn. Reson. Med.* 38(6), 874–877.